WRF Simulations of the 20–22 January 2007 Snow Events over Eastern Canada: Comparison with In Situ and Satellite Observations

J. J. SHI,*,+ W.-K. TAO,* T. MATSUI,*,+ R. CIFELLI,# A. HOU,@ S. LANG,*,& A. TOKAY,*,**
N.-Y. WANG,++ C. PETERS-LIDARD,## G. SKOFRONICK-JACKSON,*
S. RUTLEDGE,# AND W. PETERSEN@@

* *Laboratory for Atmospheres, NASA Goddard Space Flight Center, Greenbelt, Maryland*
+ *Goddard Earth Sciences and Technology Center, University of Maryland, Baltimore County, Baltimore, Maryland*
# *Department of Atmospheric Science, Colorado State University, Fort Collins, Colorado*
@ *Goddard Modeling Assimilation Office, NASA Goddard Space Flight Center, Greenbelt, Maryland*
& *Science Systems and Applications, Inc., Greenbelt, Maryland*
** *Joint Center for Earth Systems Technology, University of Maryland, Baltimore County, Baltimore, Maryland*
++ *Earth System Science Interdisciplinary Center, University of Maryland, College Park, College Park, Maryland*
Laboratory for Hydrospheric Processes, NASA Goddard Space Flight Center, Greenbelt, Maryland
@@ *Earth Sciences Office, NASA Marshall Space Flight Center, Huntsville, Alabama*

(Manuscript received 11 May 2009, in final form 7 May 2010)

ABSTRACT

One of the grand challenges of the Global Precipitation Measurement (GPM) mission is to improve cold-season precipitation measurements in mid- and high latitudes through the use of high-frequency passive microwave radiometry. For this purpose, the Weather Research and Forecasting model (WRF) with the Goddard microphysics scheme is coupled with a Satellite Data Simulation Unit (WRF–SDSU) to facilitate snowfall retrieval algorithms over land by providing a virtual cloud library and corresponding microwave brightness temperature measurements consistent with the GPM Microwave Imager (GMI). When this study was initiated, there were no prior published results using WRF at cloud-resolving resolution (1 km or finer) for high-latitude snow events. This study tested the Goddard cloud microphysics scheme in WRF for two different snowstorm events (a lake-effect event and a synoptic event between 20 and 22 January 2007) that took place over the Canadian *CloudSat*/Cloud-Aerosol Lidar and Infrared Pathfinder Satellite Observation (CALIPSO) Validation Project (C3VP) site in Ontario, Canada. The 24-h-accumulated snowfall predicted by WRF with the Goddard microphysics was comparable to that observed by the ground-based radar for both events. The model correctly predicted the onset and termination of both snow events at the Centre for Atmospheric Research Experiments site. The WRF simulations captured the basic cloud patterns as seen by the ground-based radar and satellite [i.e., *CloudSat* and Advanced Microwave Sounding Unit B (AMSU-B)] observations, including the snowband featured in the lake event. The results reveal that WRF was able to capture the cloud macrostructure reasonably well. Sensitivity tests utilizing both the ''2ICE'' (ice and snow) and ''3ICE'' (ice, snow, and graupel) options in the Goddard microphysical scheme were also conducted. The domain- and time-averaged cloud species profiles from the WRF simulations with both microphysical options show identical results (due to weak vertical velocities and therefore the absence of large precipitating liquid or high-density ice particles like graupel). Both microphysics options produced an appreciable amount of liquid water, and the model cloud liquid water profiles compared well to the in situ C3VP aircraft measurements when only grid points in the vicinity of the flight paths were considered. However, statistical comparisons between observed and simulated radar echoes show that the model tended to have a high bias of several reflectivity decibels (dBZ), which shows that additional research is needed to improve the current cloud microphysics scheme for the extremely cold environment in high latitudes, despite the fact that the simulated ice/liquid water contents may have been reasonable for both events. Future aircraft observations are also needed to verify the existence of graupel in high-latitude continental snow events.

Corresponding author address: Dr. Jainn J. Shi, Code 613.1, NASA/GSFC, Greenbelt, MD 20771.
E-mail: jainn.j.shi@nasa.gov

DOI: 10.1175/2010JAMC2282.1

1. Introduction

The NASA Global Precipitation Measurement (GPM) mission is a multinational, multisatellite mission designed to provide a uniformly calibrated precipitation measurement around the world. GPM consists of two components: a core satellite and a constellation of satellites. The core satellite carries a dual-frequency precipitation radar and a microwave radiometric imager, known as the GPM Microwave Imager (GMI), with high-frequency channels. The constellation of satellites consists of one National Aeronautics and Space Administration (NASA)-provided satellite, U.S. satellite assets from the National Oceanic and Atmospheric Administration (NOAA) and Defense Meteorological Satellite Program, and international satellites with passive microwave instruments. Two of the major objectives of the GPM mission are to measure cold-season precipitation in mid- and high latitudes over land through the use of GMI high-frequency radiometry and to further the understanding of precipitation processes at high latitudes. In 2007, the Canadian *CloudSat*/Cloud-Aerosol Lidar and Infrared Pathfinder Satellite Observation (CALIPSO) Validation Project (C3VP) field campaign took place in south-central Ontario in Canada. C3VP was a multinational, multiagency field experiment hosted by Environment Canada in and around the Centre for Atmospheric Research Experiments (CARE) about 80 km north of Toronto, Ontario. GPM's participation in C3VP was aimed at improving space-based snowfall detection and estimation algorithms (Petersen et al. 2007). In this study, the Weather Research and Forecasting model (WRF) with the Goddard microphysics scheme was utilized. WRF has also been coupled with multisensor, multifrequency satellite simulators in the Goddard Satellite Data Simulation Unit (SDSU) for model evaluation and GPM algorithm support. The goal is to combine radar, satellite, and in situ measurements in addition to model data to improve precipitation measurement. The Goddard cloud microphysics scheme in WRF is tested for two distinct snowstorm events observed over the C3VP site in Ontario between 0000 UTC 20 January and 0000 UTC 23 January 2007. Observations from the Environment Canada King City (Ontario) radar, in situ aircraft measurements, and *CloudSat* are used to validate the model simulations.

The Great Lakes of North America are unique water bodies that have a large enough surface area to inject appreciable amounts of relatively warm water vapor into passing cold Arctic air masses to produce snowstorms on the lee side of the lakes during the autumn and winter seasons. Under suitable conditions (that involve the lake–air temperature difference, airflow, and stability in the boundary layer), strong organized convection may develop. The resulting lines or bands of clouds can produce considerable amounts of snow and are known as lake-effect snowstorms. Classic storms that occur on the cold-air side of synoptic-scale systems (i.e., synoptic events) tend to occur under stable conditions, which suppress convection; however, lake enhancements of large synoptic-scale storms may also be significant, although any associated convection in this type of situation tends to be weaker than in lake-effect storms caused by passing Arctic air (Hjelmfelt 1990).

One of the snow events simulated in this study was a lake-effect system. Although the dynamics of lake-effect systems have been well studied (Brown 1972; Sykes and Henn 1989; Weckwerth et al. 1997, 1999; Kelly 1984; Cooper et al. 2000; Kristovich 1991; Tripoli 2005), little detailed research on cloud microphysical properties in lake-effect systems has been published (Schroeder et al. 2006). Schroeder et al. (2006) stated that one potentially important factor in the development of heavy snowfall in lake-effect events is the modification of lake-effect clouds and snow by seeding from higher-level cloud layers. Evidence from aircraft microphysical measurements showed that microphysical snow-growth processes were locally enhanced within the convective boundary layer (CBL) clouds in seeded regions and that the CBL was locally deeper in seeded regions than in nonseeded regions. They also analyzed ice-particle size spectra to determine the microphysical differences between seeded and nonseeded areas. Seeded spectra in all cases implied more intense snowfall than did nonseeded spectra. Because of the lack of numerical and observational studies on the microphysical properties of lake-effect systems, many questions still remain unresolved. The existence of large precipitating particles like rain or graupel in these kinds of cloud systems is unknown, as is the presence of cloud liquid water in high-latitude cold-season cloud systems during the peak of wintertime when air temperatures throughout the column are below −10°C.

Table 1 lists some post-1989 modeling studies (as well as the current one) for lake-effect snowstorms, including their cloud microphysics schemes. These studies were focused more on the dynamics associated with lake-effect snowstorms than on their microphysical properties. Maesaka et al. (2006) used a cloud-resolving model (CRM; at 0.5-km horizontal resolution) with initial and boundary conditions provided by a WRF run at 5-km horizontal resolution to simulate a high-latitude lake-effect snow event that developed over the Great Lakes in January 2003. They concluded that CRMs can produce realistic simulations of mesoscale weather systems like lake-effect snow events that develop as a result of the interaction of synoptic-scale and cloud-scale circulations in the presence of varying surface conditions.

TABLE 1. A list of numerical studies with cloud-resolving microphysics on lake-effect snowstorms.

	Modeling system	Microphysics	Resolution	Simulation time
Hjelmfelt (1990)	Colorado State University Mesoscale model (Pielke 1974, 1984; McNider and Pielke 1981)	Hjelmfelt and Braham (1983) and Mahrer and Pielke (1978)	Horizontal: 36 × 46 at 8-km resolution Vertical: levels defined at 10, 100, 500, 1000, 1500, 2000 m, etc.	20 h
Rao and Agee (1996)	Moeng–Purdue large-eddy simulation model (Moeng 1984, 1986; Moeng and Wyngaard 1988) with ice phase	Lin et al. (1983), Rutledge and Hobbs (1983), and Murakami (1990)	Horizontal 40 × 40 at 125-m resolution Vertical: 40 layers with 50-m resolution	6000 s
Ballentine et al. (1998)	Fifth-generation Pennsylvania State University–NCAR Mesoscale Model (MM5; Grell et al. 1994)	Dudhia (1989) with simplified treatment of ice and snow	Horizontal: nested domains with resolution of 135, 45, 15 and 5 km, respectively Vertical: 23 layers	36 h
Cooper et al. (2000)	University of Oklahoma Advanced Regional Prediction System (Xue et al. 1995a,b)	Lin et al. (1983) and Tao and Simpson (1993)	Horizontal: 61 × 61 at 500-m resolution Vertical: 10-m spacing near surface;200-m spacing near and above the top of PBL	6 h
Tripoli (2005)	University of Wisconsin Nonhydrostatic Mesoscale model (Tripoli 1992)	Bulk microphysics with cloud water, pristine ice crystals, aggregated crystals, and rimed crystals	Horizontal: 500 × 90 at 400 m Vertical: 100-m spacing inside lowest 1.2 km, stretched slowly to 750 m spacing by 5 km AGL	6 h
Maesaka et al. (2006)	Cloud-Resolving Storm Simulator (CReSS; Tsuboki and Sakakibara 2002)	Bulk parameterization of cold rain cloud physics with predicted ice concentration	Horizontal: 2600 × 1320 at 500 m Vertical: 40 layers, 40-m resolution near the surface and 453 m at the top of the domain	12 h
Shi et al. (this study)	WRF version 2.2.1	GCE microphysics (Tao et al. 2003; Lang et al. 2007)	Horizontal: 457 × 457 at 1 km Vertical: 61 layers	84 h

They did not nest WRF down to a cloud-resolving scale (1 km or finer), however—probably because of the significant computational resources required for such a setup (Maesaka et al. 2006). When the current study was initiated, there were no prior published results using WRF at cloud-resolving resolution (1 km or finer) for high-latitude snow events. The term ''high latitude'' is used to distinguish these events from snow events accompanying midlatitude frontal systems farther south. One of the goals of this study is to determine whether a high-resolution mesoscale model such as WRF with an advanced bulk microphysical scheme designed for CRMs can properly simulate the cloud systems and snowfall associated with high-latitude snow events occurring in continental environments.

Two Goddard cloud microphysics options [''3ICE'' (ice, snow, and graupel) and ''2ICE'' (ice and snow)] in WRF were tested for two distinct snowstorm events that were observed over the C3VP site in Ontario between 0000 UTC 20 January and 0000 UTC 23 January 2007. A brief review of WRF, the Goddard physical packages, and the satellite simulators is given in section 2. The synoptic situation for the region between 20 and 22 January 2007 is discussed in section 3. In section 4, the design of the model simulations is discussed. In section 5, results from the high-resolution WRF simulations are compared with in situ and satellite observations, including the Environment Canada King City operational dual-polarimetric radar located about 35 km southeast of the CARE site and *CloudSat*-observed reflectivities. In addition, mean cloud hydrometeor profiles from the simulations are examined. The summary and conclusions are given in section 6.

2. Brief review of WRF, the Goddard physical packages, and the satellite simulators

WRF is a next-generation mesoscale forecast model and assimilation system. The development of WRF has been a multiagency effort led by National Center for Atmospheric Research (NCAR) with several NOAA and U.S. Department of Defense partners. The model is designed to support research advancing the understanding and the prediction of mesoscale precipitation systems. It incorporates advanced numerics and data assimilation

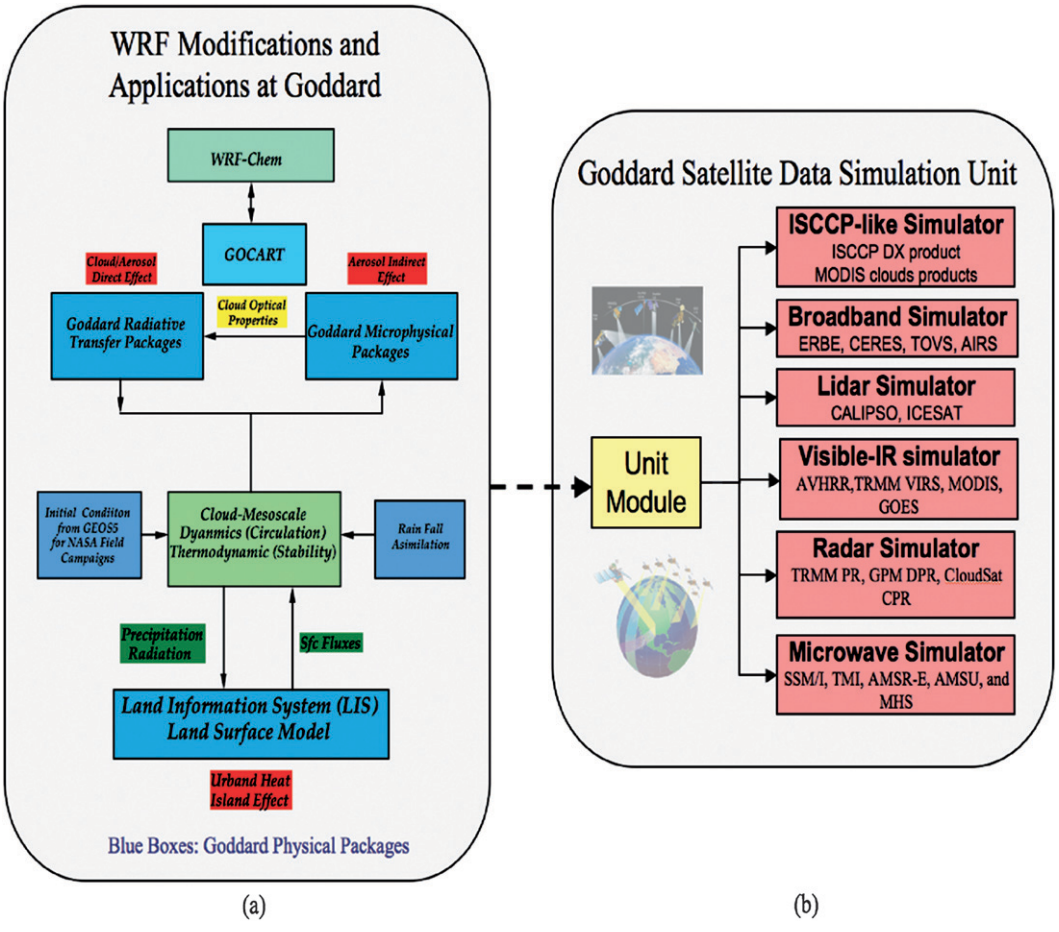

FIG. 1. (a) Physical packages added into WRF at Goddard, and (b) the Goddard SDSU.

techniques, a multiple relocatable nesting capability, and improved physics. WRF has been used for a wide range of applications, from idealized research to operational forecasting, with an emphasis on a horizontal grid in the range of 1–10 km. Its spectrum of physics and dynamics options reflects the experience and input of the broad scientific community (Michalakes et al. 2004). The WRF Software Framework (WSF) provides the infrastructure that accommodates the dynamics solvers, physics packages that interface with the solvers, and programs for initialization. There are two dynamics solvers in the WSF: the Advanced Research WRF (ARW) solver (originally referred to as the Eulerian mass or ''em'' solver), developed primarily at NCAR, and the Nonhydrostatic Mesoscale Model solver developed at the National Centers for Environmental Prediction (NCEP). Detailed documentation on WRF and the WSF can be found in Skamarock et al. (2008). In this study, the ARW version was used.

Various Goddard physical packages (i.e., CRM-type microphysics, radiation, and land surface hydrology processes) as well as a real-time forecast system using Goddard Earth Observing System global analyses being developed at NASA have recently been implemented into the WRF ARW system (Fig. 1a). The Goddard Cumulus Ensemble (GCE) model's (Tao and Simpson 1993) one-moment bulk microphysical scheme was recently implemented into WRF. This scheme is mainly based on Lin et al. (1983), with additional processes from Rutledge and Hobbs (1984). The Goddard microphysical scheme includes three different options: 3ICE-graupel, 3ICE-hail, and 2ICE (only cloud ice and snow). The Goddard microphysics scheme was recently modified to reduce overestimated and unrealistic amounts of cloud water and graupel in the stratiform region (Tao et al. 2003; Lang et al. 2007).

The Goddard radiation package includes both longwave and shortwave radiation and has been developed over the past two decades at NASA Goddard Space Flight Center for use in general circulation models, regional models, and CRMs (Chou and Suarez 1999, 2001). A few recent improvements were made to the Goddard radiation package before it was added into WRF: 1) the

shortwave radiation code was optimized for computational speed (by a factor of 2), 2) cloud optical properties were made to be consistent with the assumptions in the Goddard microphysics, 3) stratospheric layers can be optionally added above the top of the model pressure level, and 4) the aerosol direct effect on both longwave and shortwave radiation has been accounted for (Matsui et al. 2007).

The Goddard SDSU is an end-to-end multisatellite simulator unit. It has six simulators at present: passive microwave, radar, visible–infrared spectrum, lidar, International Satellite Cloud Climatology Project, and broadband. The SDSU can compute satellite-consistent radiances or backscattering signals from simulated atmospheric profiles and condensates consistent with the Goddard microphysics (Fig. 1b). For example, it can generate estimates of retrieved microphysical quantities that can be directly compared with high-resolution satellite (i.e., TRMM and *CloudSat*) products. These simulated radiances and backscattering can be directly compared with satellite observations, establishing a satellite-based framework for evaluating the cloud parameterizations. This method is superior to the traditional method of validating models with satellite-based products, because models and satellite products often use different assumptions in their cloud microphysics (Matsui et al. 2009). Once the cloud model reaches satisfactory agreement with the satellite observations, simulated clouds, precipitation, atmospheric states, and satellite-consistent radiances or backscattering can be made available as an a priori database for developing physically based cloud and precipitation retrieval algorithms. Thus, the SDSU coupled with the multiscale modeling system can allow us to understand cloud processes better as well as to improve precipitation retrievals from current and future NASA satellite missions (Matsui et al. 2008).

3. Synoptic conditions

There were two significant snow events during the 72-h period from 0000 UTC 20 January to 0000 UTC 23 January 2007. Height, temperature, and wind analyses at 850 hPa from the NCEP North American Mesoscale (NAM) model with a 25-km horizontal resolution are shown Fig. 2. On 20 January 2007, a cold front passed the Toronto area from the north in association with an upper-level trough centered over eastern Canada (Figs. 2a–c). The passage of the cold front produced strong northwesterly flow in the lower troposphere, which allowed for the development of isolated snowbands over Lake Huron and in the lee of Georgian Bay and Lake Huron. A series of northwest–southeast-oriented snowbands developed over the CARE site (44.23°N, 79.78°W) after 0000 UTC 20 January. Although the bands persisted throughout the day, observations from the nearby King City radar (located at 43.96°N, 79.57°W) showed that they were most intense prior to 0600 UTC (isolated cores exceeding 30 dBZ) with echo tops below about 3 km AGL. Figure 3a shows the 24-h accumulation of snowfall [liquid water equivalent (LWE) in millimeters] derived from the nearby King City radar observations. The method for deriving the LWE snowfall from the King City radar is described in Huang et al. (2010). Most of the intense snowfall was between Lake Huron and the CARE site, with the 24-h-accumulated snowfall ranging from 2 to 12.5 mm. Daily accumulations measured from the double-fenced international reference (DFIR) gauge at the CARE site indicated approximately 12.3 mm of LWE for the event, which was the highest daily amount observed for the entire 2006/07 season (Bringi et al. 2008). This value (~12.3 mm) is in excellent agreement with the radar estimate (~12.5 mm) for the CARE site shown in Fig. 3a. Although terrain was not a factor in the formation of the snowbands, which occurred out over the lake, it could have played a role farther downwind, but the surrounding area is relatively flat with a maximum elevation of only a few hundred meters. Because the snowfall in this first event was mainly caused by the passage of cold air over the relatively warm lake, this event is hereinafter called the *lake event*.

In contrast to the lake event on 20 January, the second snow event on 22 January was the result of a synoptic-scale system moving across southern Ontario. The 22 January event developed in response to the passage of a 500-hPa short-wave trough and an associated surface low (Figs. 2e,f) from west to east across the C3VP domain between 0000 and 1200 UTC (Petersen et al. 2007). The winds were relatively calm and the air temperatures were relatively warm in comparison with the lake event that occurred 2 days earlier. This synoptic-scale system was associated with widespread light-to-moderate snowfall (Fig. 3b). King City radar data showed that precipitation entered the western portion of the inner (1 km) domain around 1500 UTC 21 January. The precipitation initially weakened considerably as the system moved eastward and northeastward. However, radar imagery showed that a weak mesoscale snowband propagated northward in the vicinity of the CARE site and interacted with the larger-scale system after about 2100 UTC 21 January. The combined system continued to move eastward and left the C3VP domain after 0800 UTC 22 January. Range–height indicator scans from the King City radar indicated that echo tops extended up to about 5.5 km AGL, with reflectivities mostly below 25 dBZ. Surface temperatures during this event were well below freezing, from −9° to −10°C, and rawinsonde data collected during the event indicated near-water-saturated conditions (and

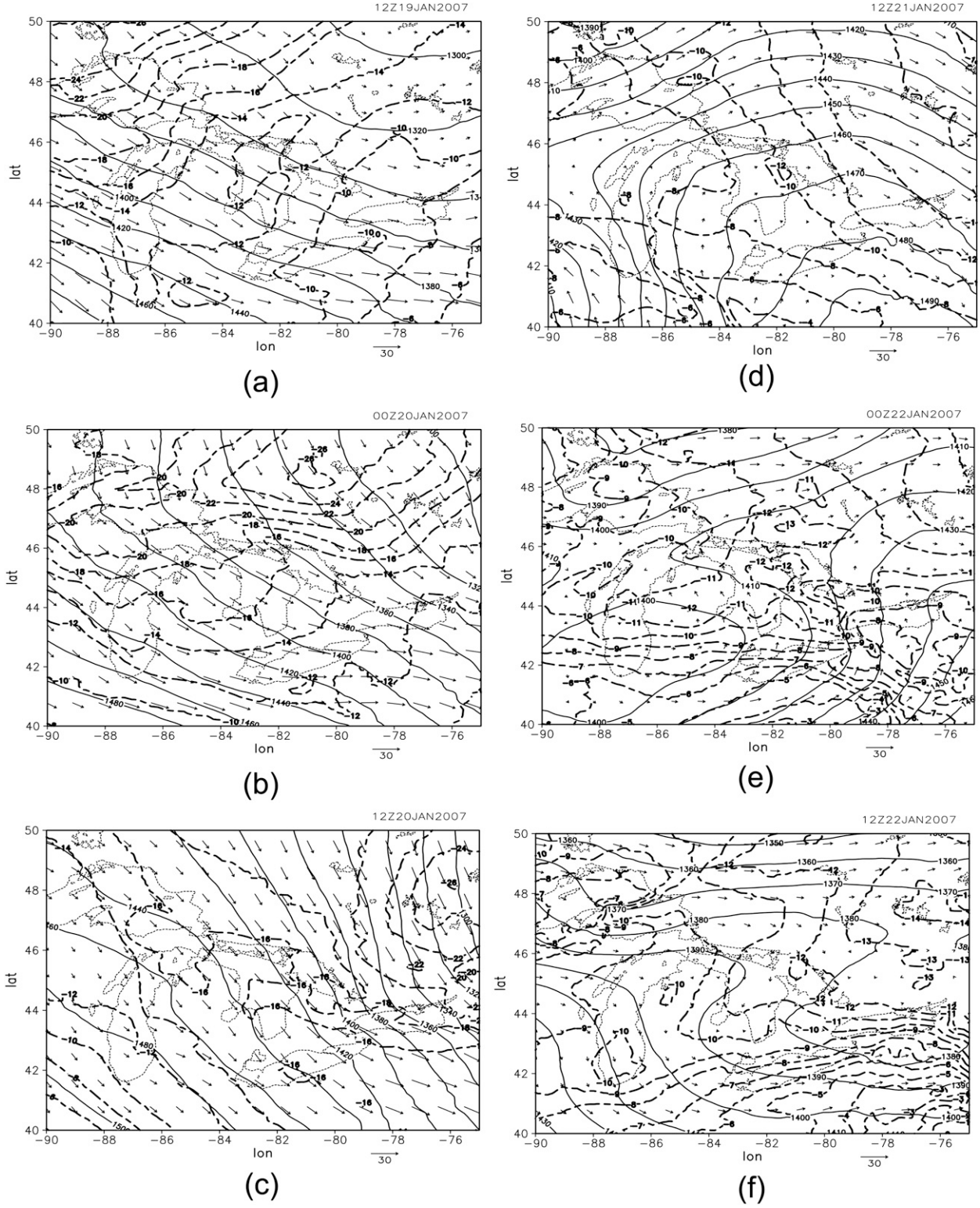

FIG. 2. The 850-hPa heights (solid contours; m), temperatures (dashed contours; °C), and winds (vectors; m s^{-1}) from NCEP NAM 25-km analyses for the lake event at (a) 1200 UTC 19 Jan, (b) 0000 UTC 20 Jan, and (c) 1200 UTC 20 Jan, and for the synoptic event at (d) 0000 UTC 21 Jan, (e) 0000 UTC 22 Jan, and (f) 1200 UTC 22 Jan 2007.

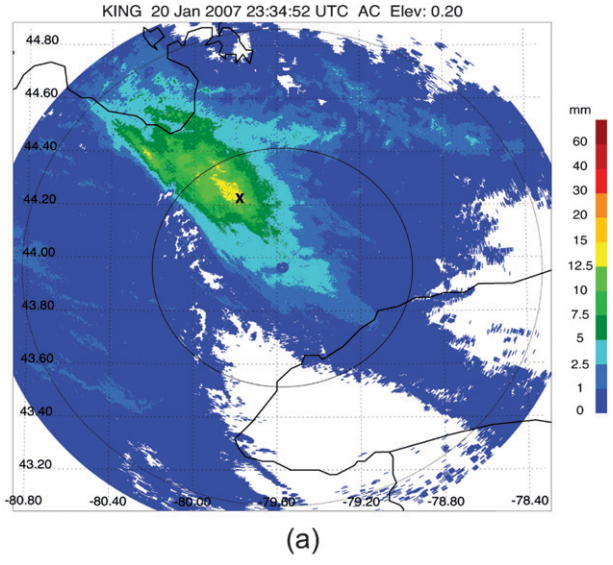

FIG. 3. The 24-h-accumulated snowfall (mm; liquid water equivalent) derived from the nearby King City radar observations for (a) the lake event (0000 UTC 20 Jan–0000 UTC 21 Jan) and (b) the synoptic event (1200 UTC 21 Jan–1200 UTC 22 Jan). The "X" denotes the location of the CARE site.

definitely ice-supersaturated conditions) in the first several kilometers of the sounding. Winds were generally moderate at the surface, on the order of 5 m s^{-1}, for the duration of the event. The DFIR gauge at the CARE site reported about 2.4 mm of 24-h-accumulated LWE in association with this event (Bringi et al. 2008). This event is hereinafter called the *synoptic event*.

4. Model setup

NASA's interest in the C3VP project was primarily to support snowfall retrievals over land using high-frequency

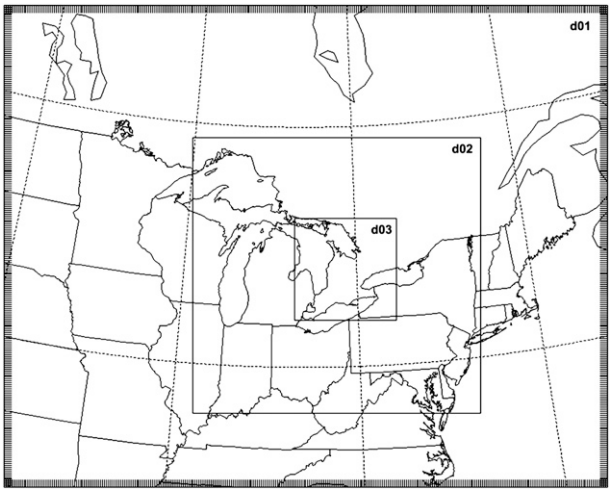

FIG. 4. Nesting configuration used for the C3VP simulations. Horizontal resolutions for domains 1, 2, and 3, are 9, 3, and 1 km, respectively.

radiometer observations through a set of ground- and aircraft-based instrumental and remote sensing measurements as well as high-resolution numerical modeling. During the winter of 2006/07, a number of in situ and remote sensing precipitation measuring instruments were operated at the CARE site located near Egbert, Ontario, about 30 km to the northwest of the King City C-band operational dual-polarized radar. While the experiment was originally designed to measure winter precipitation for C3VP, NASA's GPM ground validation program joined the effort (Petersen et al. 2007) by bringing 2D-video and Particle Size and Velocity (PARSIVEL) disdrometers and a multifrequency radar to the CARE site. To examine the cloud dynamics and microphysical properties of the snowstorms, WRF, version 2.2.1, with the Goddard microphysical scheme was used to conduct the simulations. In this study, only the 3ICE-graupel and 2ICE options were used with WRF.

Double-nested domains were constructed with horizontal grid spacings of 9, 3, and 1 km and corresponding grids of 301 × 241, 430 × 412, and 457 × 457 for the outer, middle, and inner domains, respectively (Fig. 4). A terrain-following vertical coordinate with 61 layers was constructed with resolutions ~5–10 hPa inside the PBL and ~20–25 hPa above the PBL. Time steps of 30, 10, and 3.333 s were used in the outer and two nested grids, correspondingly. The coarse domain extended from Nebraska to Nova Scotia, Canada, and from North Carolina to the northern end of Ontario, while the finest domain covered most of southeastern Ontario as well as most of Lakes Huron and Erie (Fig. 4). The model was initialized from NCEP Global Forecast System (GFS) analyses with 1° resolution. Time-varying lateral boundary

conditions also from the NOAA/NCEP global analyses were provided at 6-h intervals. The model was integrated for 48 h twice, from 1200 UTC 19 January to 1200 UTC 21 January and from 0000 UTC 21 January to 0000 UTC 23 January 2007, respectively, for both snow events.

The Grell–Dévényi ensemble cumulus parameterization scheme (Grell and Dévényi 2002) was used for the coarse 9-km grid domain. The cumulus parameterization scheme was turned off in the 3- and 1-km grid domains while the Goddard cloud microphysics scheme was used in all three grid domains. The Goddard longwave and shortwave schemes recently added into WRF, and discussed in section 2, were adopted to provide longwave and shortwave parameterizations that interact with the atmosphere. The planetary boundary layer parameterization for this study was the Mellor–Yamada–Janjić (Mellor and Yamada 1982; coded and modified by Dr. Janjić for the NCEP Eta Model) level-2 turbulence closure model for the full range of atmospheric turbulent regimes. The surface heat and moisture fluxes (from both ocean and land) were computed from similarity theory (Monin and Obukhov 1954). The "Noah" (from NCEP–Oregon State University–U.S. Air Force–National Weather Service Office of Hydrologic Development) land surface model was used, which is based on Chen and Dudhia (2001). It is a four-layer soil temperature and moisture model with canopy moisture and snow cover prediction. It provides sensible and latent heat fluxes to the boundary layer scheme. The soil temperature and moisture were also initialized from NCEP GFS analyses.

5. Results

a. Snowfall comparison

Figure 5 shows the 24-h-accumulated LWE snowfall (mm) from the inner (1 km) domain of the WRF output for the lake event (Fig. 5a) and the synoptic event (Fig. 5b). For a better comparison with Fig. 3, Figs. 5a and 5b are centered on the King City radar site (43.96°N, 79.57°W). Both figures have 201 grid points (200 km) in the longitude and latitude directions, similar to the 100-km radius used in Fig. 3. Figures 3a and 5a show the LWE of the 24-h-accumulated snowfall (between 0000 UTC 20 January and 0000 UTC 21 January 2007) from the King City radar observations and the WRF simulations, respectively, for the lake event, and Figs. 3b and 5b show the same thing for the 24-h period from 1200 UTC 21 January to 1200 UTC 22 January 2007 for the synoptic event. For both the lake and synoptic events, the 1-km domain with the Goddard microphysics produced a maximum amount of snowfall across the region that is comparable to that observed [based on the algorithm in Huang et al. (2010)] by the King City radar: 12.5–15-mm LWE for the lake event and 2.5–5-mm LWE for the synoptic event. The DFIR gauge at the CARE site also indicated approximately 12.3 mm of snowfall for the lake event on 20 January 2007 (Bringi et al. 2008). However, the heavy-snowfall region in the model simulation for the lake event is about 0.2° longitude west of the one

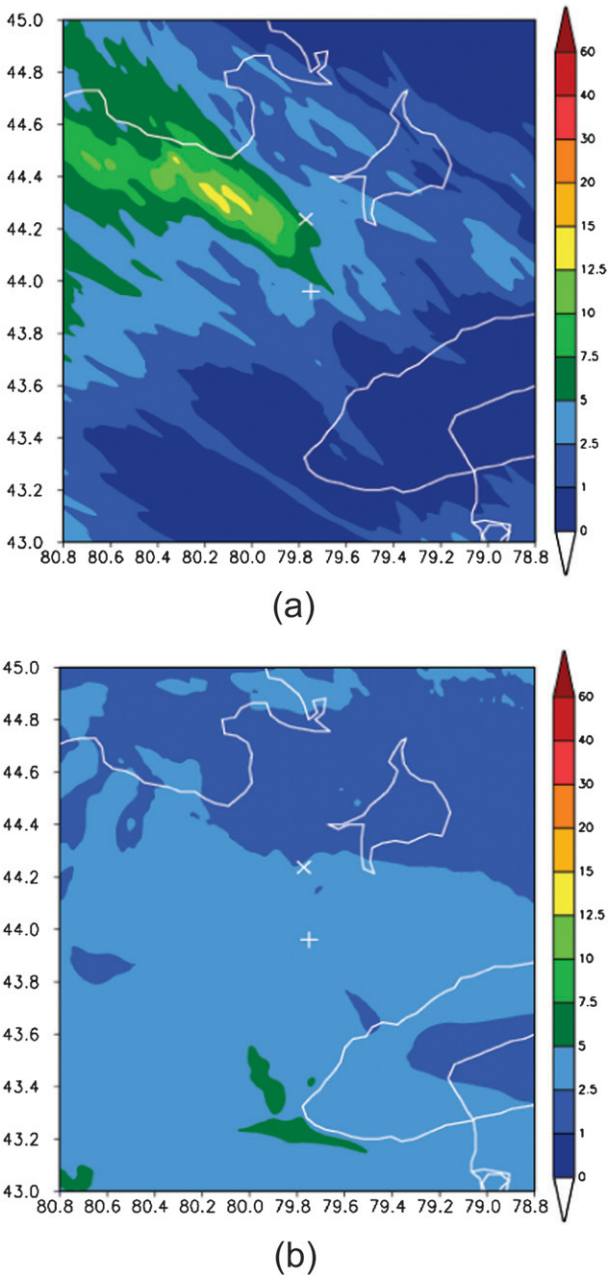

FIG. 5. WRF-simulated 24-h-accumulated snowfall (mm; liquid water equivalent) for the (a) lake event (0000 UTC 20 Jan–0000 UTC 21 Jan) and (b) synoptic event (1200 UTC 21 Jan–1200 UTC 22 Jan). The "X" denotes the location of the CARE site, and the plus sign is the location of the King City radar.

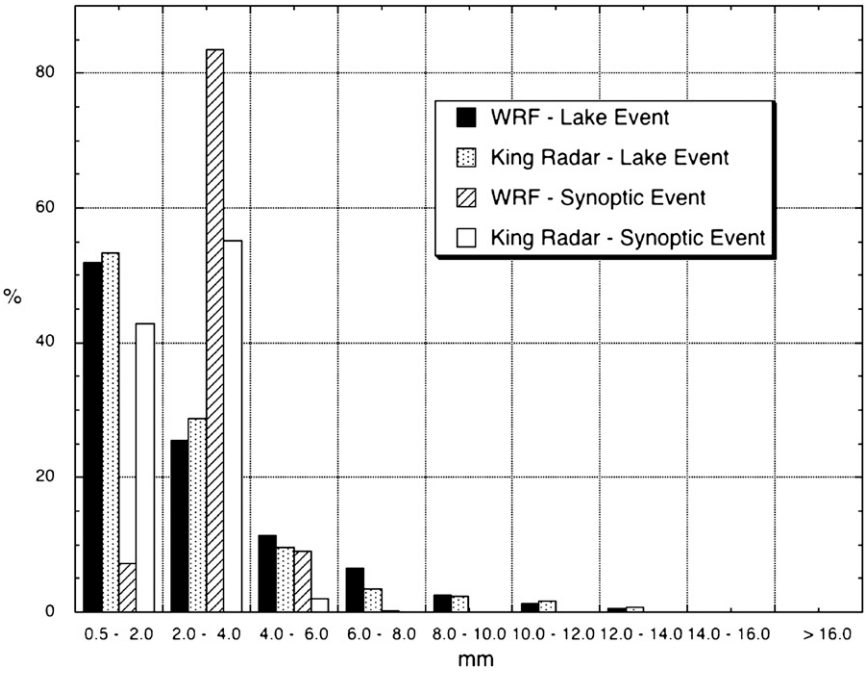

FIG. 6. PDF of 24-h-accumulated snowfall (liquid water equivalent). Results for the lake event were based on the data shown in Figs. 2a and 4a, and results for the synoptic event were based on the data shown in Figs. 2b and 4b.

shown in the King City radar observations. For the synoptic event, the 1-km domain also had a slightly larger area of LWE snowfall amounts in the range of 5–7.5 mm west of Lake Ontario than did the King City radar observations, which showed only some isolated locations with 5–7.5-mm LWE just west of the CARE site. The King City radar may have underestimated the snowfall in the region west of Lake Ontario because low-topped clouds here would be very far from the radar. Note also that radar snowfall retrievals, just like any other satellite and radar retrievals, are still not perfect. However, with current technology, this is probably the best that can be obtained for a regional snowfall estimate as opposed to a single-point snowfall estimate like the PARSIVEL (laser optical) disdrometer at the CARE site. Details on the uncertainties in the snowfall estimates from the King City radar can be found in Huang et al. (2010).

Probability density functions (PDFs) of 24-h-accumulated snowfall (LWE) from both the model simulations and the King City radar observations are shown in Fig. 6. The model results were calculated using data from all of the grid points in the 1-km domain. The results reveal that the 24-h-accumulated snowfall predicted by the model agrees well with the radar observations over the whole spectrum for the lake event. For the synoptic event, most of the snowfall predicted by the model is in the 2.0–4.0-mm range (more than 80%) while most of the snowfall observed by the King City radar is in the 0.5–2.0- (43%) and 2.0–4.0-mm (55%) range. Only 2% of the grid points from the radar had snowfall in the 4.0–6.0-mm range, with none larger than 6.0 mm, whereas around 10% of the grid points for the model had snowfall in the 4.0–6.0-mm range. Overall, both the model and the King City radar had nearly a 10% probability of having snowfall amounts greater than 6.0 mm LWE for the lake event and virtually no grids with snowfall larger than 6.0 mm for the synoptic event. This confirms that the synoptic event produced a much more uniformly distributed snowfall across the region whereas the lake event produced areas of heavy snowfall within the snowbands.

Figure 7 shows the 72-h time series of snowfall rates (mm h^{-1}) at the CARE site (44.23°N, 79.78°W) for the period from 0000 UTC 20 January to 0000 UTC 23 January 2007. Figure 7a represents the data collected from the PARSIVEL (laser optical) disdrometer stationed at the CARE site, and Fig. 7b represents the model simulation at the same location. As shown in Fig. 7, the heavy snowfall at the CARE site for the lake event started around 0300 UTC and ended around 0700 UTC with light snowfall throughout the rest of 20 January. For the synoptic event, snow started at 0200 UTC and ended around 0800 UTC 22 January. A comparison of Figs. 7a and 7b shows that the onset and ending times predicted by the model agree well with the observations,

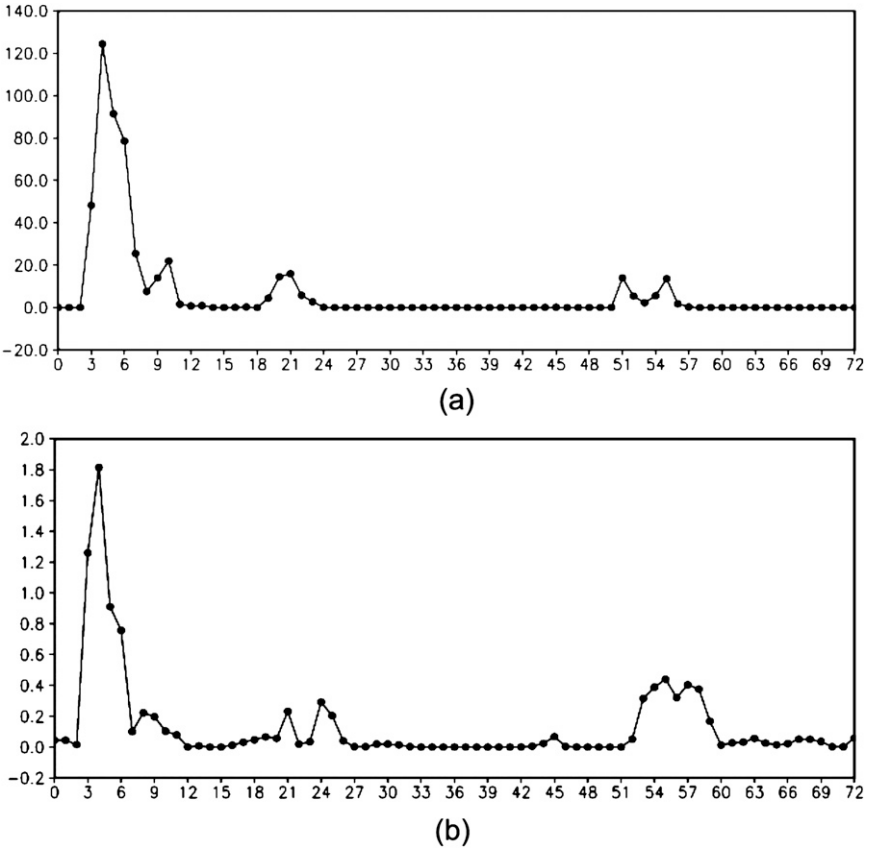

FIG. 7. (a) Snowfall rate (mm h^{-1}; dry snow) collected from the PARSIVEL (laser optical) disdrometer at the CARE site, and (b) the corresponding WRF-simulated snowfall rate (mm h^{-1}; liquid water equivalent) between 0000 UTC 20 Jan and 0000 UTC 23 Jan 2007.

as do the predicted times of peak snowfall. As pointed out in Bringi et al. (2008), the snow that fell at the CARE site during the lake event was particularly dry, with densities possibly between 0.06 and 0.08 g cm^{-3}. For a lake-effect snow event in a very cold atmosphere, it is very common for the snow-to-liquid ratio to range from 12:1 to 25:1 (Baxter et al. 2005; Milbrandt et al. 2009). However, even with a 25:1 snow-to-liquid ratio, the snowfall predicted by the model for the lake event is still weaker than that observed by the PARSIVEL disdrometer. However, this result is easily understandable when comparing Figs. 3 and 5. The model-predicted intense-snowfall region is about 0.2° longitude west of the CARE site, which resulted in the model not predicting any heavy snowfall directly over the CARE site.

Overall, the amount of accumulated snowfall predicted by the model across the region agrees well with the King City radar observations in both events, with the exception that the model did not predict intense snowfall at the CARE site. The model did, however, correctly predict the onset and termination of both snow events as shown in the PARSIVEL disdrometer observations at the CARE site. Although the model did not predict the correct snowfall rate at the CARE site for the lake event, it is extremely difficult to predict an accurate precipitation amount at a single-point location in a high-resolution mesoscale model; alternative methods such as the composite-based method used in Nachamkin et al. (2005) may be required for evaluation.

b. Reflectivity comparison

For the lake event (Fig. 8), the snowband simulated by the model is in good agreement with the observed snowband in terms of the timing and the overall location; however, the observed band seems to be oriented more north–south, and the model-predicted C-band reflectivities are about 10 dBZ stronger than those from the King City radar. The observed echo tops reach to around 3.5 km, whereas those in the model only reach to around 2.5 km. In addition, the radar-observed snowband appears to be more consolidated (i.e., with a large continuous core) with a varying depth, whereas the model-simulated band depicts multiple small-scale cores of nearly constant depth. The radar-observed snowband is deepest close to the lake

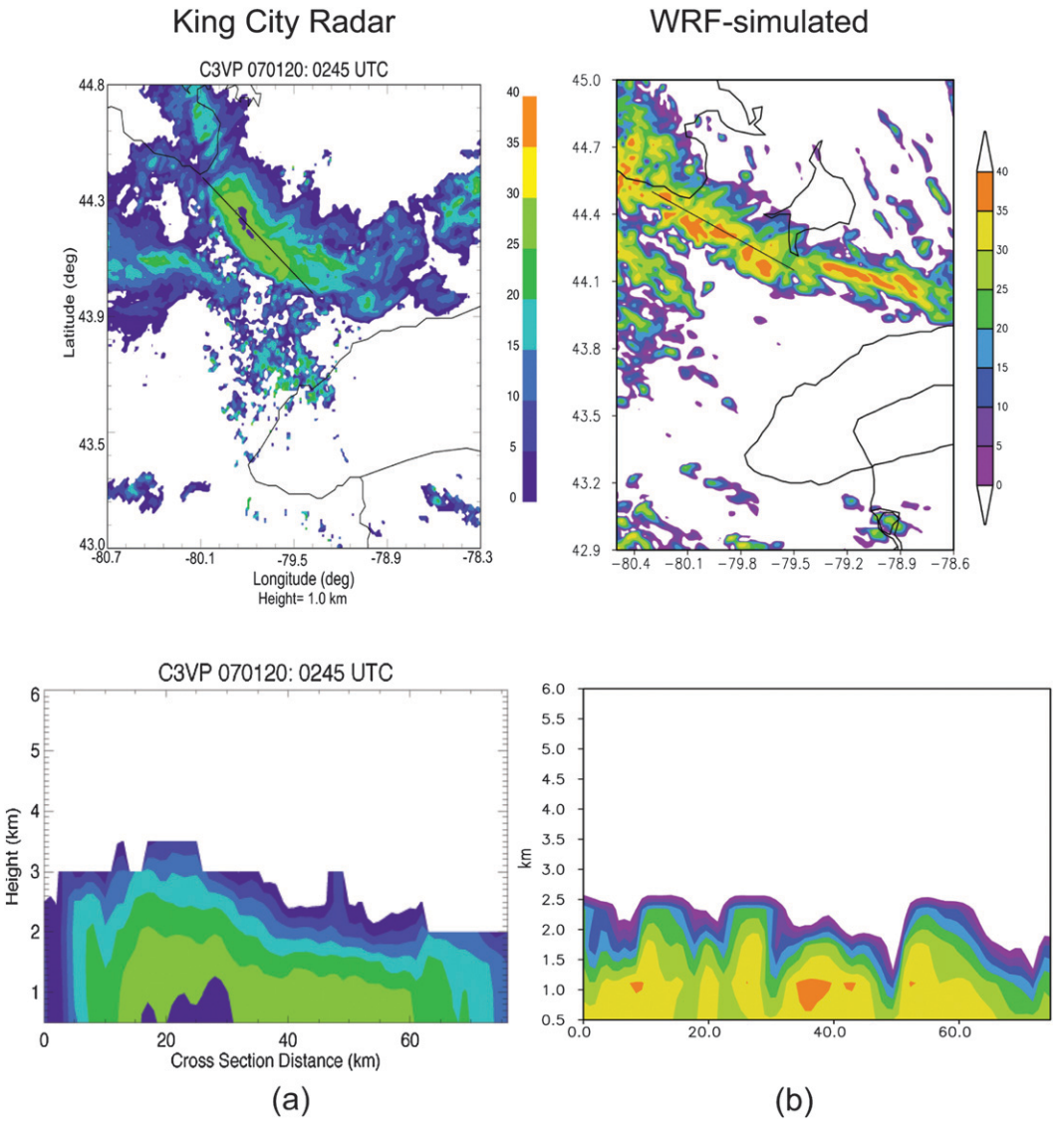

FIG. 8. Radar reflectivities from (a) the King City radar and (b) simulated by WRF for the lake-effect event. (top) Radar reflectivity at a height of 1 km centered on the King City radar site (43.96°N, 79.57°W). Slanted lines show the location of the (bottom) corresponding radar reflectivity cross sections. Note that there is a jump in the King City radar reflectivities from 25 to 0 dBZ below ~1.2 km between 20 and 30 km as seen in (a). This effect is due to the removal of ground clutter.

(Fig. 8a). Although the only available *CloudSat* pass occurred nearly 5 h later (0745 UTC on the same day), *CloudSat*-observed radar (94 GHz) reflectivities also confirm the presence of echoes with 3.5-km tops (see pass 1 in Fig. 10). Because the targeted cloud band was very narrow, other nearby parallel cross sections also show similar results.

Figure 9 shows that the model-simulated C-band radar reflectivities for the synoptic event are also in good agreement with the observed reflectivities in terms of the strength and vertical structure. However, the model-simulated reflectivity pattern shows a larger area of moderate values (>20 dBZ) than does the observed pattern. Both the model and observed reflectivity cross sections show radar echoes extending to around 4 km, except for a few spikes that go above 4 km in the observed reflectivity cross section.

Figure 10 displays W-band radar reflectivities from the *CloudSat* Cloud Profiling Radar (CPR). Simulated W-band radar reflectivities are calculated from the radar simulator (Masunaga and Kummerow 2005) in the SDSU using the WRF results from along the exact same path as the *CloudSat* overpass. Pass 1 represents the lake event, and passes 2 and 3 represent the early and late stages of

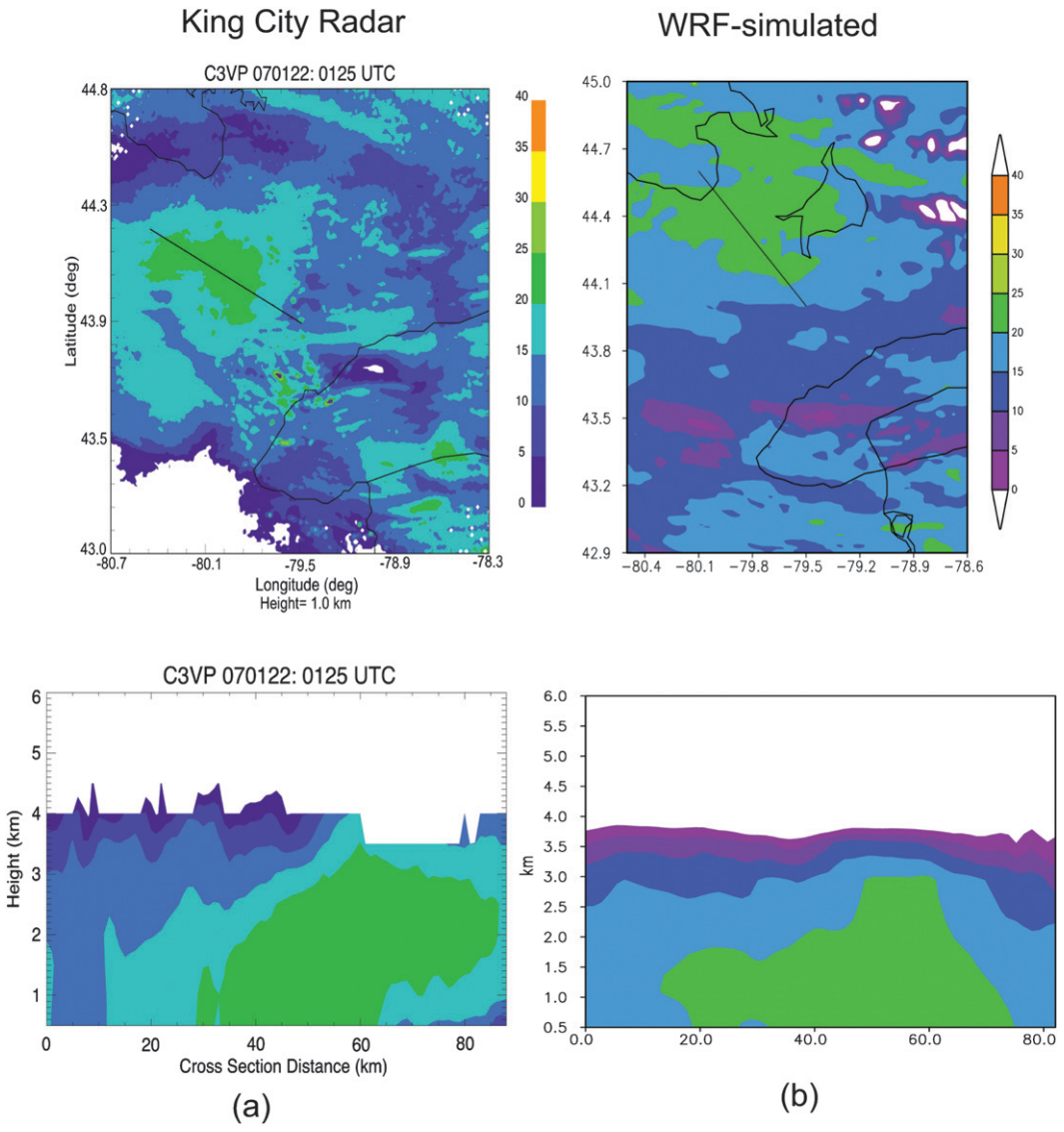

FIG. 9. As in Fig. 8, but for the synoptic event.

the synoptic event. Note that WRF output is produced every model hour because of its volumetric size, which results in a time difference of 30 min or less with the overpass data. The cross-sectional comparison indicates that WRF successfully captured the basic horizontal and vertical patterns of radar reflectivities associated with the shallow echoes in pass 1, the deeper and broader echoes associated with large-scale nimbostratus in pass 2, and the multilayer echoes in pass 3. The model-simulated echoes were deeper than what was observed by *CloudSat* along the entire cross section in pass 2, especially in the area over Lake Huron in the northern part of the model domain.

To perform a systematic evaluation of the overall quality of the model results, contoured-frequency-with-altitude diagrams (CFAD; Yuter and Houze 1995) of radar echo data were constructed. CFADs of radar echo give a graphic depiction of the frequency distribution of radar echoes in each vertical layer. To construct the plots, the data were stratified by altitude only, without regard to the horizontal locations. A comparison of the CFADs from the WRF–SDSU-simulated radar echoes with those from the *CloudSat* observations (Fig. 11) reveals that statistically WRF significantly overestimated the intensity of radar reflectivities above 2.5 km in pass 3 and above 1 km in pass 2 but especially below 5 km, where 4 dBZ occurred at more than 40% of the grid points in the WRF innermost domain. In pass 1, the distributions of WRF-simulated radar reflectivity are more comparable to the *CloudSat* distributions, except that the WRF distributions

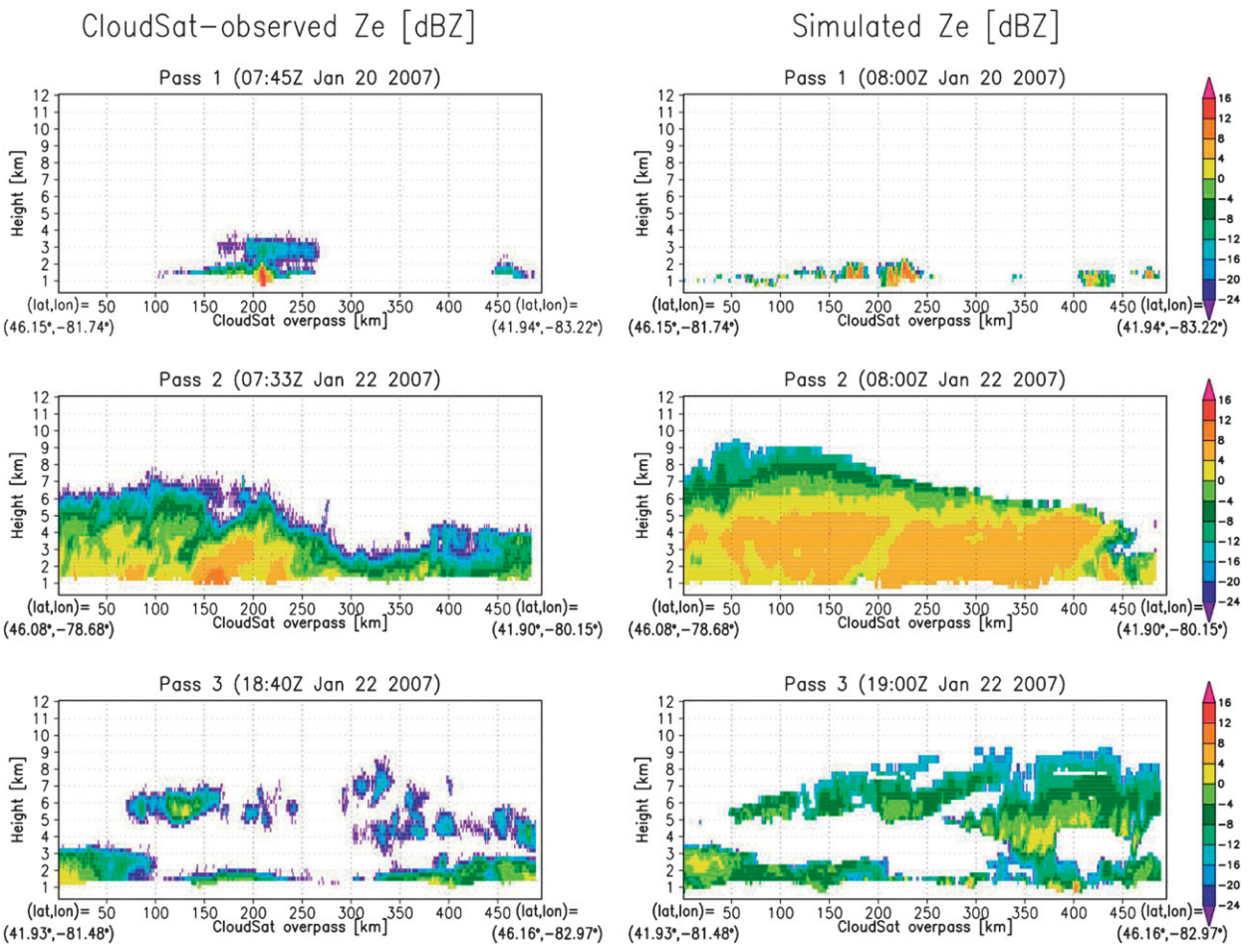

FIG. 10. Instantaneous cross sections of *CloudSat*-observed and WRF–SDSU-simulated CPR (94 GHz) reflectivity. (left) *CloudSat* observations from three different passes, and (right) the corresponding WRF values.

are capped at around 2.5 km whereas the *CloudSat* distributions, although weak, extend to 3.5 km. Also, the model misses the peak at 12 dBZ in the lowest level. These results suggest that WRF with the Goddard one-moment bulk microphysics scheme was able to capture the cloud macrostructure reasonably well but not the cloud microphysical structure.

c. *Brightness temperature comparison*

Model-simulated high-frequency microwave brightness temperatures (Tb) corresponding to the Advanced Microwave Sounding Unit B (AMSU-B) sensors were also derived from the model simulations. The AMSU-B sensors were originally designed for temperature and humidity profile retrievals. However, these high-frequency channels (150.00, 183.31 ± 1, 183.31 ± 3, and 183.31 ± 7 GHz) were found to be sensitive to falling snow and relatively insensitive to ground signals. Therefore, they are useful for snowfall retrievals over land (Skofronick-Jackson et al. 2004). It is planned to include such high-frequency channels on the GMI to support snowfall retrievals over land at mid- and high latitudes. This makes the simulation and evaluation of high-frequency Tb from WRF an important focus for supporting the GPM mission. AMSU-B-consistent Tb were computed from the WRF simulations through a passive microwave simulator in the SDSU (using delta-Eddington two-stream radiative transfer with slant path view; Kummerow 1993; Olson and Kummerow 1996). AMSU-B Tb (within the 30° sensor-viewing angle) and corresponding Tb simulated from the WRF simulation were sampled consistently in time (±30 min) and space (instantaneous field of view = 16.4 km at nadir).

A total of 10 AMSU-B swaths were matched, containing 1738 and 2958 Tb samples over water and land, respectively (Fig. 12). These were then used to evaluate the simulated cold-cloud systems for various Tb. The largest discrepancy (RMSE of 10.2°K over water and 9.93°K over land) between the observations and the simulations is for

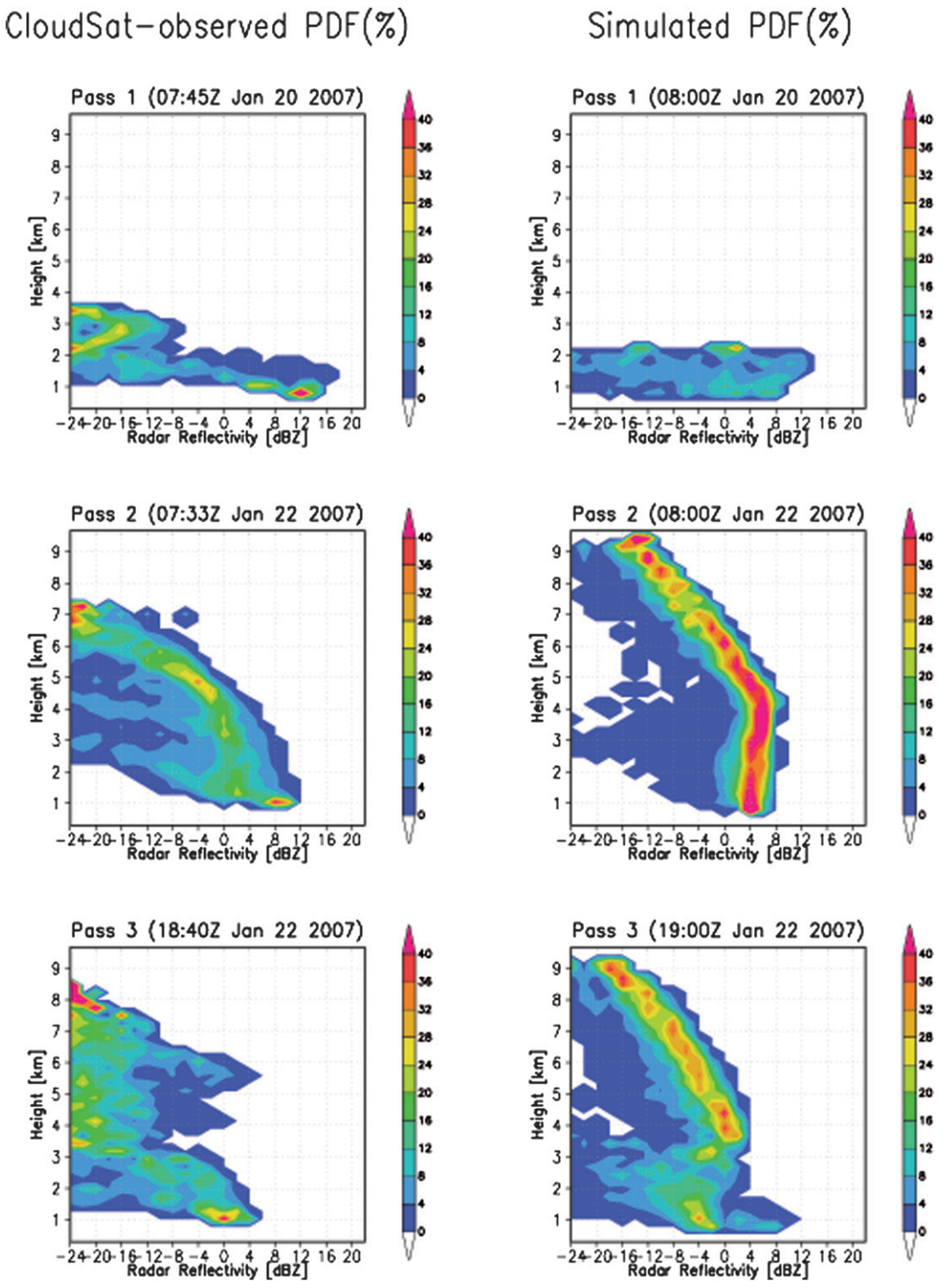

FIG. 11. Instantaneous CFADs of *CloudSat*-observed and WRF–SDSU-simulated CPR (94 GHz) reflectivity. (left) *CloudSat* observations from three different passes, and (right) the results from the WRF simulations. Color shading represents the percentage of occurrence of dB*Z* values.

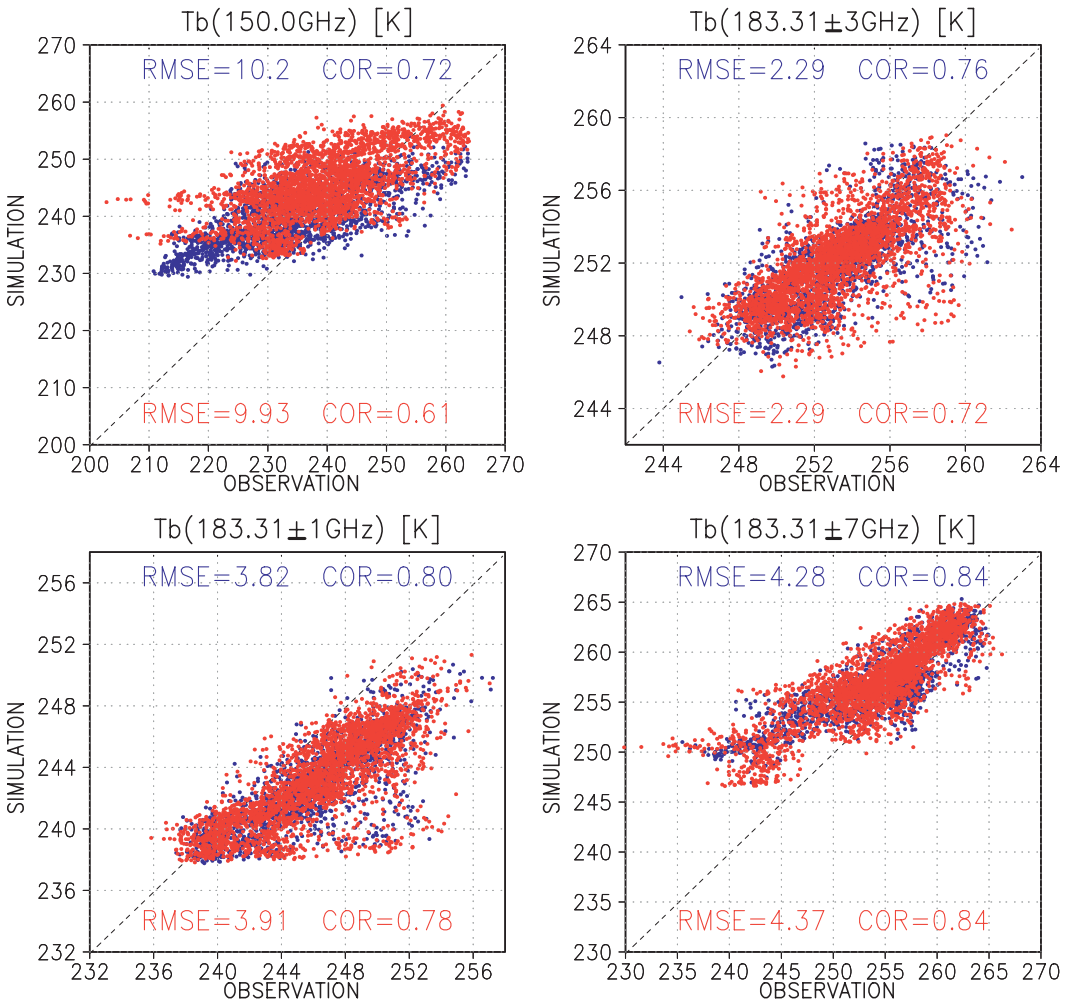

FIG. 12. Scatterplots of AMSU-B-observed and WRF–SDSU-simulated Tb at different high-frequency channels. Red (blue) points represent overland (overwater) points. Root-mean-square error (RMSE) and correlation (COR) are also displayed.

the 150-GHz Tb because of uncertainties in the simulated surface properties (e.g., skin temperature and surface emissivity), which are currently not well parameterized in the SDSU. The 180.31 ± 1 GHz and 180.31 ± 3 GHz Tb have stronger water absorption channels; hence simulated Tb are essentially unaffected by surface properties. As a result, Tb between the observations and the simulations are more consistent. The 180.31 ± 7 GHz Tb have the highest correlation (0.84) among the different channels. It is interesting to note that the model tends to overestimate the 150-GHz and 180.31 ± 7 GHz Tb (where the atmosphere is more transparent) and to underestimate the Tb of other channels (where the atmosphere is less transparent). This suggests that there might be discrepancies between the simulated and actual temperature and humidity profiles. Chaboureau and Pinty (2006) showed that their microphysical scheme could better capture the observed upper-tropospheric humidity when the ice-to-snow autoconversion threshold used in the scheme was reevaluated using a brightness-temperature-difference technique. Additional model simulations with higher-resolution and improved microphysics as well as a better representation of surface characteristics will be conducted in the near future.

d. Vertical profiles of simulated cloud species

Vertical profiles of the domain- and time-averaged cloud species from WRF using the Goddard 3ICE-graupel option are shown in Fig. 13. Only results from the Goddard 3ICE-graupel option are shown because the Goddard 2ICE option produced identical vertical profiles. For the lake event (Fig. 13a), there were no large precipitating liquid (rain) or high-density ice (graupel) particles because the simulated vertical velocities were weak (~50 cm s^{-1})

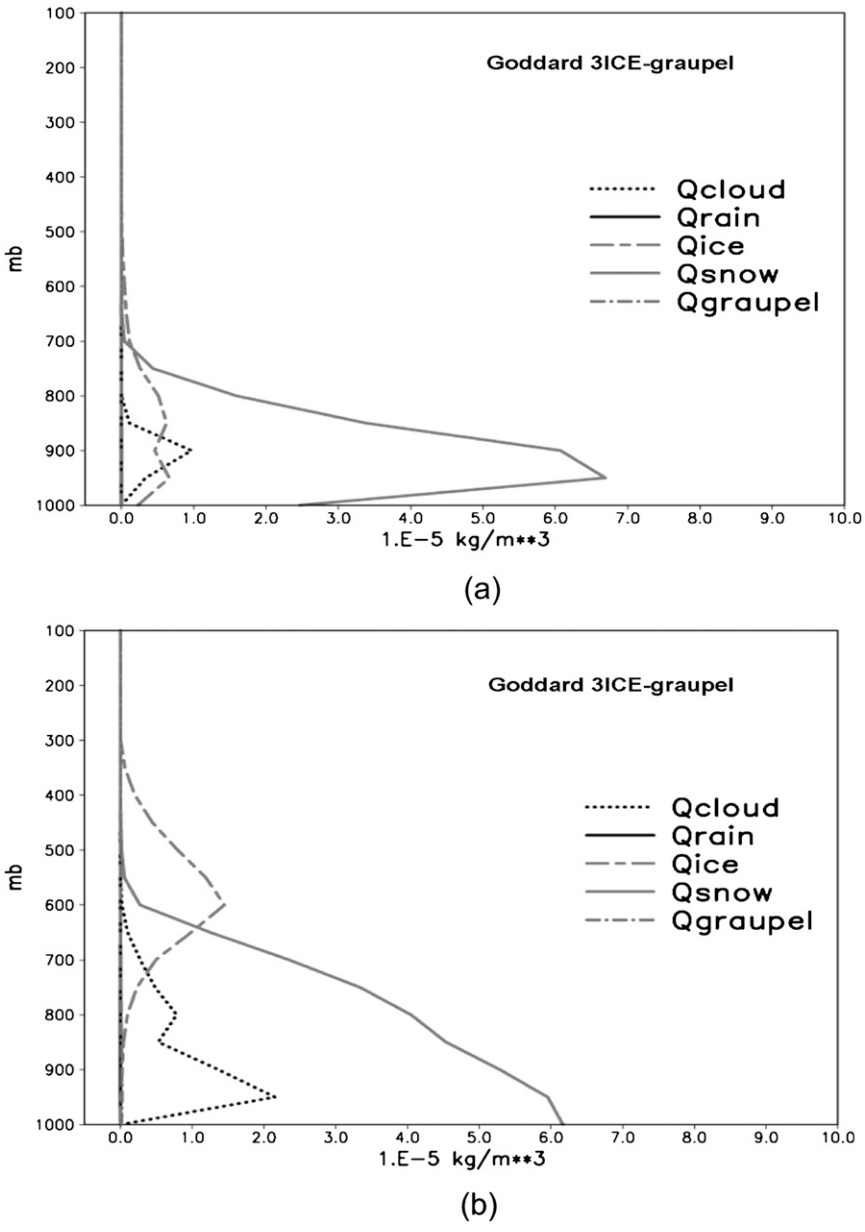

FIG. 13. WRF-simulated vertical profiles of domain-averaged and 24-h time-averaged cloud species (i.e., cloud water, rain, cloud ice, and snow) using the Goddard 3ICE-graupel scheme for the (a) lake event and the 24-h period from 0000 UTC 20 Jan to 0000 UTC 21 Jan 2007 and (b) synoptic event and the 24-h period from 0000 UTC 22 Jan to 0000 UTC 23 Jan 2007.

and the temperatures were extremely cold (see Fig. 15). The hydrometeor profiles for both the 3ICE-graupel and 2ICE experiments were identical even though the 3ICE-graupel scheme contains physics that allows the production of graupel. Also of note is the presence of cloud liquid water, despite this being a snow event; this has been observed and simulated in other studies (e.g., a snow event over the Japan Sea; Masataka et al. 2002). C3VP aircraft observations suggested that there was a little liquid water present in the lake event (A. Heymsfield 2009, personal communication). The fact that none of the cloud species extend above 700 hPa in the lake event suggests it was mostly a PBL phenomenon, which is consistent with many past studies (Kristovich 1993; Weckwerth et al. 1999; Cooper et al. 2000; Tripoli 2005).

Domain- and time-averaged profiles of cloud species for the synoptic event are presented in Fig. 13b. As with the lake event, the Goddard 3ICE-graupel and 2ICE

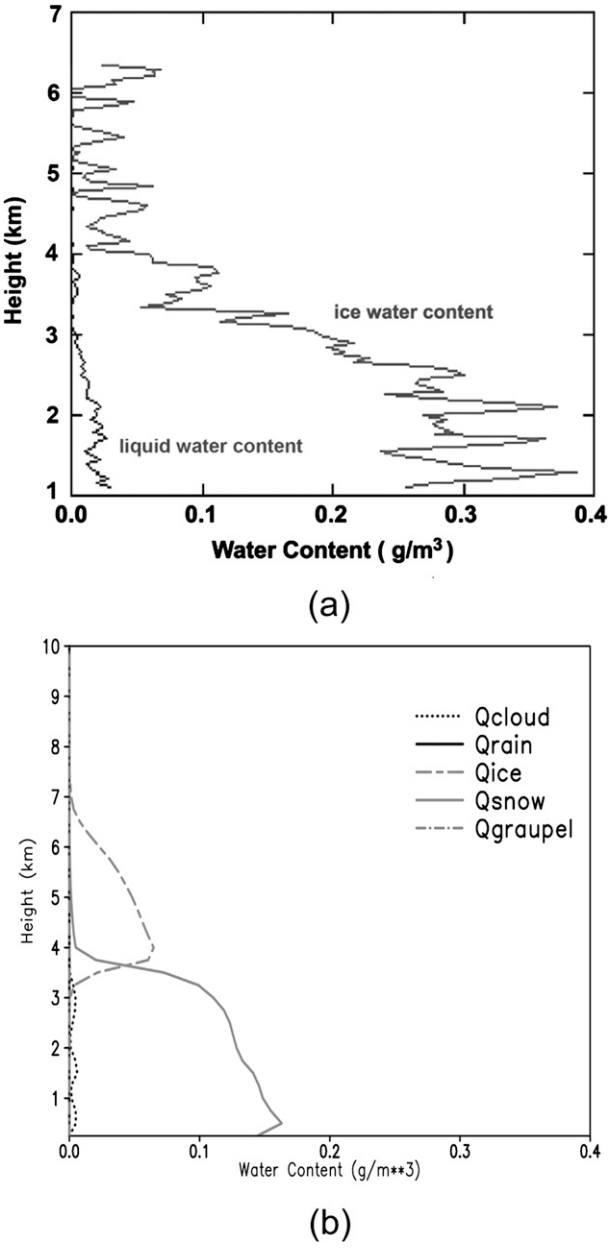

FIG. 14. (a) Vertical profiles of the C3VP aircraft-measured ice and liquid water contents between 0600 and 0624 UTC 22 Jan 2007. The vertical axis represents heights above mean sea level. (b) Vertical profiles of area-averaged cloud species (using only grid points in the vicinity of the aircraft flight path) from the model for the period between 0600 and 0700 UTC 22 Jan 2007.

simulations produced identical vertical profiles without any rain or graupel. Both options produced much snow below 500 hPa and a moderate amount of cloud ice between 400 and 700 hPa. Both options also produced a significant amount of cloud liquid water below 600 hPa. The net amount of cloud water (Qcloud) production is about one-fourth of that for snow (Qsnow) at 900 hPa, whereas it is only about one-tenth as much in the C3VP aircraft observations near a height of 1 km (Fig. 14a). However, comparing 24 min of aircraft observations with 24 h of domain-averaged model output (Fig. 13b) may not be appropriate. To provide a more direct comparison, vertical profiles of area-averaged cloud species were calculated using only grid points in the vicinity of the flight path that were close in time (i.e., between 0600 and 0700 UTC 22 January 2007) to the aircraft sampling period (Fig. 14b). Although the model only produced (net) about one-half of the snow shown in the aircraft profile below a height of 2 km, it produced (net) very little liquid water over the area as well. A comparison of Figs. 14a and 14b shows that the liquid-to-ice water ratio for the model is similar to that for the aircraft measurements below 2 km. The main reason the WRF domain-averaged profiles (Fig. 13b) appeared to contain an excessive amount of liquid water relative to the aircraft measurements was that the aircraft flight path, which was mostly around the CARE site, did not sample the entire WRF domain, which had a significantly larger amount of cloud liquid water in the southern one-third of the domain.

Figure 15 shows north–south cross sections of temperature and ice content (cloud ice plus snow) from the model along a longitude of ~79.5°W for both events. Air temperatures were very cold (<−9°C in the lake event and <−6°C in the synoptic event) throughout the column. Figure 15 shows that the simulated ice structures for the lake and synoptic events are distinctly different. The lake event contains shallow, localized areas of high ice content, whereas the synoptic event has broader, deeper areas of moderate ice contents, which is consistent with the simulated reflectivity patterns. This type of synthetic data can be valuable for snow retrieval algorithm development but only if the synthetic data can be validated with quality observational data.

6. Summary and future work

One of the grand challenges of the GPM mission is to improve cold-season precipitation measurements in mid- and high latitudes through the use of high-frequency passive microwave radiometry. In support of this objective, WRF with the Goddard microphysics scheme was coupled with the SDSU to facilitate snowfall retrieval algorithms over land by providing a virtual cloud library, including corresponding synthetic Tb that are consistent with the GMI. This study tested two different options (2ICE and 3ICE-graupel) of the Goddard cloud microphysics scheme within WRF for two snow events that took place over the C3VP site in Ontario, Canada, between 20 and 22 January 2007. When this study was initiated,

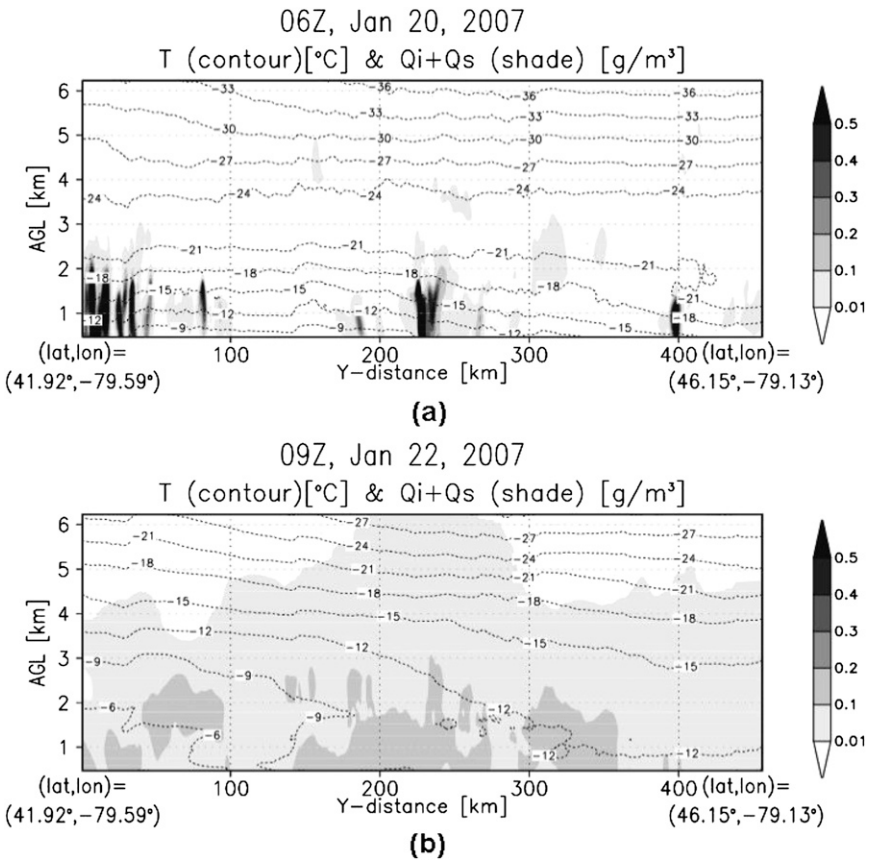

FIG. 15. Vertical cross sections of WRF-simulated temperature (°C) and cloud ice plus snow amounts (g m^{-3}) for the (a) lake and (b) synoptic events.

there were no prior published results using WRF at cloud-resolving resolution (1 km or finer) for high-latitude snow events. This study has demonstrated the feasibility of using WRF in this very mode.

The 24-h-accumulated snowfall predicted by WRF with the Goddard microphysics was comparable to the King City radar-observed accumulated snowfall for both events. However, WRF failed to predict the intense snowfall observed at the CARE site because the intense-snowfall region simulated in WRF was roughly 0.2° west of that observed by the King City radar. A PDF analysis of the accumulated snowfall amounts showed that WRF agreed well with the King City radar estimates for both events. The model correctly predicted the onset and end of both snow events at the CARE site, although it did not predict the correct snowfall rate at the CARE site because it is extremely difficult to predict the precipitation amount at a single-point location in a high-resolution mesoscale model.

In this study, corresponding radar reflectivities simulated by WRF were compared with radar and satellite observations. The comparisons indicated that WRF was able to capture the basic cloud patterns observed by ground-based radar and satellite (i.e., *CloudSat* and AMSU-B), including the snowband associated with the lake event. However, the model was found to underpredict the echo-top heights for the lake event. An additional sensitivity test using a different PBL scheme failed to resolve this bias. WRF did, however, capture the basic horizontal and vertical structures of each of the events, including the two-layer cloud structure observed during the late stage of the synoptic event. Statistical comparisons between observed and simulated radar echoes using CFAD analyses showed that the model tended to have a positive bias of several dB*Z* units When taken collectively, these results suggest that WRF was able to capture the cloud macrostructure reasonably well, but not the cloud microphysical structure. All numerical simulations suffer from errors as a result of numerical truncation, imperfect physical parameterizations, and imperfect initial and boundary conditions. At the moment, it is not clear what caused the model radar echoes to have a shallow bias for the lake event and a deep bias for the synoptic event. There are several possible reasons

for the positive bias in the overall echo intensities evident in the CFAD comparisons: the simulated snow amounts were too large, the assumed snow densities were too high, the particle sizes were too large, or a combination of these factors. More detailed dynamic and microphysical studies are required to address these issues in the future. One possible improvement that has been under development is to vary the intercept parameters for the size distribution of snow as a function of temperature.

The Goddard 3ICE-graupel and 2ICE options produced identical vertical profiles of cloud hydrometeors for the lake event with neither producing any rain or graupel, because of the cold temperatures and weak simulated vertical velocities. The same was true for the synoptic event. Although the model suggests that there was no graupel in either the lake or the synoptic event because of the weak vertical velocities in these events, there were no observations to confirm this. Future aircraft observations are needed to verify the existence of graupel in high-latitude inland snow events and to document the frequency and seasonal distribution of graupel in high-latitude inland snow events. Comparisons between vertical profiles of aircraft-measured and model-simulated ice and liquid water contents suggest that the model appeared to have simulated a reasonable amount of cloud liquid water for the synoptic event. The fact that the simulated snowbands were relatively shallow in the lake event suggests that it was mostly a PBL phenomenon, which is consistent with many past studies (Kristovich 1993; Weckwerth et al. 1999; Cooper et al. 2000; Tripoli 2005).

An improved version of the one-moment bulk microphysics scheme is now being developed based largely on the radiance-based model evaluations conducted here and the C3VP aircraft in situ observations of microphysical properties (A. Heymsfield 2009, personal communication). The intercept parameters for the size distribution of snow and graupel, which are constant values in the current scheme, will both be made a function of temperature. In addition, finer spatial resolutions than the current 1-km horizontal grid spacing may be required to represent the evolution of vigorous cold-cloud systems realistically. Model simulations with improved microphysics are necessary to provide consistent 4D thermodynamic and dynamic cloud datasets for future GPM snow retrievals and to improve our understanding of precipitation processes over high-latitude regions.

Model data are often used to infer critical cloud information/properties that are not directly observable by satellites. The linkage between the satellite and model usually depends on the simulated Tb. As such, an accurate vertical distribution of modeled cloud species is important for satellite retrievals. Unrealistic precipitation ice (i.e., snow and/or graupel) contents, particle size distributions, or particle densities can bias the simulated Tb and reflectivities, making it difficult to infer cloud properties from remote sensing data via the model. Accurate depictions of cloud ice and cloud water are also important in the model for cloud–radiation interaction. Future research will be conducted using a finer vertical resolution (both in the lower and upper troposphere) and a further-improved microphysics scheme to look further into the sensitivity of the PBL processes. Future WRF simulations may also benefit from initial and lateral boundary conditions obtained from NCEP NAM 218 grids at 12-km resolution when they become available at either the National Climatic Data Center or NCAR. Also, a WRF–Earth satellite simulator with realistic ground emissivity is required to improve the passive microwave simulator in the SDSU.

Acknowledgments. The WRF–Goddard cloud microphysics coupling is supported by the NASA Headquarters Atmospheric Dynamics and Thermodynamics Program and the NASA Tropical Rainfall Measuring Mission (TRMM). The authors are grateful to Dr. R. Kakar at NASA Headquarters for his support of this research. The authors also appreciate their useful discussion with Dr. Andy Heymsfield of NCAR.

REFERENCES

Ballentine, R. J., A. J. Stamm, and E. E. Chermack, 1998: Mesoscale model simulation of the 4–5 January 1995 lake-effect snowstorm. *Wea. Forecasting,* **13,** 893–920.

Baxter, M. A., C. E. Graves, and J. T. Moore, 2005: A climatology of snow-to-liquid ratio for the contiguous United States. *Wea. Forecasting,* **20,** 729–744.

Bringi, V. N., G.-J. Huang, D. Hudak, R. Cifelli, and S. Rutledge, 2008: A methodology to derive radar reflectivity–liquid equivalent snow rate relations using C-band radar and a 2D video disdrometer. *Extended Abstracts, Fifth European Conf. on Radar in Meteorology and Hydrology,* Helsinki, Finland, Finnish Meteorological Institute. [Available online at http://erad2008.fmi.fi/proceedings/extended/erad2008-0070-extended.pdf.]

Brown, R. A., 1972: On the inflection point instability of a stratified Ekman boundary layer. *J. Atmos. Sci.,* **29,** 850–859.

Chaboureau, J.-P., and J.-P. Pinty, 2006: Validation of a cirrus parameterization with Meteosat Second Generation observations. *Geophys. Res. Lett.,* **33,** L03815, doi:10.1029/2005GL024725.

Chen, F., and J. Dudhia, 2001: Coupling an advanced land surface–hydrology model with the Penn State–NCAR MM5 modeling system. Part I: Model implementation and sensitivity. *Mon. Wea. Rev.,* **129,** 569–585.

Chou, M.-D., and M. J. Suarez, 1999: A solar radiation parameterization for atmospheric studies. NASA Tech. Rep. NASA/TM-1999-10460, Vol. 15, 38 pp.

——, and ——, 2001: A thermal infrared radiation parameterization for atmospheric studies. NASA/TM-2001-104606, Vol. 19, 55 pp.

Cooper, K. A., M. R. Hjelmfelt, R. G. Derickson, D. A. R. Kristovich, and N. F. Laird, 2000: Numerical simulation of transitions in boundary layer convective structures in a lake-effect snow event. *Mon. Wea. Rev.,* **128,** 3283–3295.

Dudhia, J., 1989: Numerical study of convection observed during the Winter Monsoon Experiment using a mesoscale two-dimensional model. *J. Atmos. Sci.,* **46,** 3077–3107.

Grell, G. A., and D. Dévényi, 2002: A generalized approach to parameterizing convection combining ensemble and data assimilation techniques. *Geophys. Res. Lett.,* **29,** 1693, doi:10.1029/2002GL015311.

——, J. Dudhia, and D. R. Stauffer, 1994: A description of the fifth-generation Penn State/NCAR Mesoscale Model (MM5). NCAR Tech. Note TN-398STR, 122 pp.

Hjelmfelt, M. R., 1990: Numerical study of the influence of environmental conditions on lake-effect snowstorms over Lake Michigan. *Mon. Wea. Rev.,* **118,** 138–150.

——, and R. R. Braham Jr., 1983: Numerical simulation of the airflow over Lake Michigan for a major lake-effect snow event. *Mon. Wea. Rev.,* **111,** 205–219.

Huang, G.-J., V. N. Bringi, R. Cifelli, D. Hudak, and W. A. Petersen, 2010: A methodology to derive radar reflectivity–liquid equivalent snow rate relations using C-band radar and a 2D video disdrometer. *J. Atmos. Oceanic Technol.,* **27,** 637–651.

Kelly, R. D., 1984: Horizontal roll and boundary-layer interrelationships observed over Lake Michigan. *J. Atmos. Sci.,* **41,** 1816–1826.

Kristovich, D. A. R., 1991: The three-dimensional flow fields of boundary layer rolls observed during lake-effect snowstorms. Ph.D. thesis, University of Chicago, 182 pp.

——, 1993: Mean circulations of boundary-layer rolls in lake-effect snow storms. *Bound.-Layer Meteor.,* **63,** 293–315.

Kummerow, C., 1993: On the accuracy of the Eddington approximation for radiative transfer in the microwave frequencies. *J. Geophys. Res.,* **98,** 2757–2765.

Lang, S., W.-K. Tao, R. Cifelli, W. Olson, J. Halverson, S. Rutledge, and J. Simpson, 2007: Improving simulations of convective systems from TRMM LBA: Easterly and westerly regimes. *J. Atmos. Sci.,* **64,** 1141–1164.

Lin, Y.-L., R. D. Farley, and H. D. Orville, 1983: Bulk parameterization of the snow field in a cloud model. *J. Climate Appl. Meteor.,* **22,** 1065–1092.

Maesaka, T., G. W. K. Moore, Q. Liu, and K. Tsuboki, 2006: A simulation of a lake effect snowstorm with a cloud resolving numerical model. *Geophys. Res. Lett.,* **33,** L20813, doi:10.1029/2006GL026638.

Mahrer, Y., and R. A. Pielke, 1978: A test of an upstream spline interpolation technique for the advective terms in a numerical mesoscale model. *Mon. Wea. Rev.,* **106,** 818–830.

Masataka, M., M. Hoshimoto, N. Orikasa, H. Horie, H. Okamoto, H. Kuroiwa, H. Minda, and K. Nakmura, 2002: Inner structures of snow bands associated with the Japan Sea polar-airmass convergence zone based on aircraft observations. Preprints, *Int. Conf. on Mesoscale Convective Systems and Heavy Rainfall/Snowfall in East Asia,* Tokyo, Japan.

Masunaga, H., and C. D. Kummerow, 2005: Combined radar and radiometer analysis of precipitation profiles for a parametric retrieval algorithm. *J. Atmos. Oceanic Technol.,* **22,** 909–929.

Matsui, T., W.-K. Tao, and R. Shi, 2007: Goddard radiation and aerosol direct effect in Goddard WRF. *NASA/UMD WRF Workshop,* College Park, Maryland, NASA and University of Maryland, College Park, 12 pp. [Available online at http://www.atmos.umd.edu/~martini/wrfchem/ppt/WRF_Toshi.ppt.]

——, and Coauthors, 2008: Goddard Satellite Data Simulation unit: A comprehensive multi-sensor satellite simulators for supporting satellite missions. *AGU 2008 Fall Meeting,* San Francisco, CA, Amer. Geophys. Union, A21D-0268.

——, X. Zeng, W.-K. Tao, H. Masunaga, W. S. Olson, and S. E. Lang, 2009: Evaluation of long-term cloud-resolving model simulations using satellite radiance observations and multifrequency satellite simulators. *J. Atmos. Oceanic Technol.,* **26,** 1261–1274.

McNider, R. T., and R. A. Pielke, 1981: Diurnal boundary layer development over sloping terrain. *J. Atmos. Sci.,* **38,** 2198–2212.

Mellor, G. L., and T. Yamada, 1982: Development of a turbulence closure model for geophysical fluid problems. *Rev. Geophys. Space Phys.,* **20,** 851–875.

Michalakes, J., J. Dudhia, D. Gill, T. Henderson, J. Klemp, W. Skamarock, and W. Wang, 2004: The Weather Research and Forecast Model: Software architecture and performance. *Proc. 11th ECMWF Workshop on the Use of High Performance Computing in Meteorology,* Reading, United Kingdom, ECMWF, 18 pp. [Available online at http://www.ecmwf.int/newsevents/meetings/workshops/2004/high_performance_computing-11th/pdf/John_Michalakes.pdf.]

Milbrandt, J. A., D. Jacob, and R. McTaggart-Cowan, 2009: Forecasting the solid-to-liquid ratio of precipitation a cloud-resolving model. *19th Conf. on Numerical Weather Prediction,* Omaha, NE, Amer. Meteor. Soc., 7A.2. [Available online at http://ams.confex.com/ams/pdfpapers/154287.pdf.]

Moeng, C.-H., 1984: A large-eddy-simulation model for the study of planetary boundary-layer turbulence. *J. Atmos. Sci.,* **41,** 2052–2062.

——, 1986: Large-eddy simulation of a stratus-topped boundary layer. Part I: Structure and budgets. *J. Atmos. Sci.,* **43,** 2886–2900.

——, and J. C. Wyngaard, 1988: Spectral analysis of large-eddy simulations of the convective boundary layer. *J. Atmos. Sci.,* **45,** 3573–3587.

Monin, A. S., and A. M. Obukhov, 1954: Basic laws of turbulent mixing in the surface layer of the atmosphere (in Russian). *Contrib. Geophys. Inst. Acad. Sci. USSR,* **151,** 163–187.

Murakami, M., 1990: Numerical modeling of dynamic and microphysical evolution of an isolated convective cloud—The 19 July 1981 CCOPE cloud. *J. Meteor. Soc. Japan,* **68,** 107–127.

Nachamkin, J. E., S. Chen, and J. Schmidt, 2005: Evaluation of heavy precipitation forecasts using composite-based methods: A distributions-oriented approach. *Mon. Wea. Rev.,* **133,** 2163–2177.

Olson, W. S., and C. D. Kummerow, 1996: Simulated retrieval of precipitation profiles from TRMM Microwave Imager and precipitation radar data. Preprints, *Eighth Conf. on Satellite Meteorology and Oceanography,* Atlanta, GA, Amer. Meteor. Soc., 248–251.

Petersen, W. A., and Coauthors, 2007: NASA GPM/PMM participation in the Canadian CloudSat/Calipso Validation Project (C3VP): Physical process studies in snow. Preprints, *33rd Int. Conf. on Radar Meteorology,* Cairns, QLD, Australia, Amer. Meteor. Soc., P12A.8. [Available online at http://ams.confex.com/ams/pdfpapers/123652.pdf.]

Pielke, R. A., 1974: A three-dimensional numerical model of the sea breezes over south Florida. *Mon. Wea. Rev.,* **102,** 115–139.

——, 1984: *Mesoscale Meteorological Modeling*. Academic Press, 599 pp.

Rao, G.-S., and E. M. Agee, 1996: Large eddy simulation of turbulent flow in a marine convective boundary layer with snow. *J. Atmos. Sci.,* **53,** 86–100.

Rutledge, S. A., and P. V. Hobbs, 1983: The mesoscale and microscale structure and organization of clouds and precipitation in midlatitude cyclones. VIII: A model for the ''seeder-feeder'' process in warm-frontal rainbands. *J. Atmos. Sci.,* **40,** 1185–1206.

——, and ——, 1984: The mesoscale and microscale structure and organization of clouds and precipitation in midlatitude cyclones. XII: A diagnostic modeling study of precipitation development in narrow cold-frontal rainbands. *J. Atmos. Sci.,* **41,** 2949–2972.

Schroeder, J. J., D. A. R. Kristovich, and M. R. Hjelmfelt, 2006: Boundary layer and microphysical influences of natural cloud seeding on a lake-effect snowstorm. *Mon. Wea. Rev.,* **134,** 1842–1858.

Skamarock, W. C., and Coauthors, 2008: A description of the advanced research WRF version 3. NCAR Tech. Note NCAR/TN-475+STR, 88 pp.

Skofronick-Jackson, G. M., M.-J. Kim, J. A. Weinamn, and D.-E. Chang, 2004: A physical model to determine snowfall over land by microwave radiometry. *IEEE Trans. Geosci. Remote Sens.,* **42,** 1047–1058.

Sykes, R. I., and D. S. Henn, 1989: Large-eddy simulation of turbulent sheared convection. *J. Atmos. Sci.,* **46,** 1106–1118.

Tao, W.-K., and J. Simpson, 1993: The Goddard Cumulus Ensemble model. Part I: Model description. *Terr. Atmos. Oceanic Sci.,* **4,** 19–54.

——, and Coauthors, 2003: Microphysics, radiation and surface processes in the Goddard Cumulus Ensemble (GCE) model. *Meteor. Atmos. Phys.,* **82,** 97–137.

Tripoli, G. J., 1992: A nonhydrostatic mesoscale model designed to simulate scale interaction. *Mon. Wea. Rev.,* **120,** 1342–1359.

——, 2005: Numerical study of the 10 January 1998 lake-effect bands observed during Lake-ICE. *J. Atmos. Sci.,* **62,** 3232–3249.

Tsuboki, K., and A. Sakakibara, 2002: Large-scale parallel computing of cloud resolving storm simulator. *High Performance Computing,* P. Z. Hans et al., Eds., Springer, 243–259.

Weckwerth, T. M., J. W. Wilson, R. M. Wakimoto, and N. A. Crook, 1997: Horizontal convective rolls: Determining the environmental conditions supporting their existence and characteristics. *Mon. Wea. Rev.,* **125,** 505–526.

——, T. W. Horst, and J. W. Wilson, 1999: An observational study of the evolution of horizontal convective rolls. *Mon. Wea. Rev.,* **127,** 2160–2179.

Xue, M., K. K. Droegemeier, and V. Wong, 1995a: The advanced regional prediction system and real-time storm-scale weather prediction. Preprints, *Int. Workshop on Limited-Area and Variable Resolution Models,* Beijing, China, WMO and Amer. Meteor. Soc.

——, ——, ——, A. Shapiro, and K. Brewster, 1995b: ARPS version 4.0 user's guide. Center for Data Analysis and Prediction of Storms, 380 pp. [Available from the Center of Data Analysis and Prediction of Storms, University of Oklahoma, Norman, OK 73072.]

Yuter, S. E., and R. A. Houze Jr., 1995: Three-dimensional kinematic and microphysical evolution of Florida cumulonimbus. Part II: Frequency distributions of vertical velocity, reflectivity, and differential reflectivity. *Mon. Wea. Rev.,* **123,** 1941–1963.